Contents lists available at ScienceDirect

International Journal of Pharmaceutics

journal homepage: www.elsevier.com/locate/ijpharm





Effect of orientation angle for needle-free jet injection

Idera Lawal, Daniel de Castro Araujo Valente, Emil Khusnatdinov, Brian Elliott, Breanna Carruth, Clayton Penttila, Jeremy Marston*

Department of Chemical Engineering, Texas Tech University, Lubbock, TX 79409, United States of America

ARTICLE INFO

Keywords: Jet injection Needle-free Hydrogel Ex-vivo

ABSTRACT

In this paper, we report on the delivery efficiency of needle-free jet injections using injectors with typical jet speed $v_j \approx 140$ m/s, orifice diameter $d_o = 157$ µm, and volume V = 0.1 mL. The target substrates were either hydrogel tissue phantoms or porcine tissues combined with excised human skin. The novelty of this study is two-fold: First, we investigate the influence of injection angle relative to the skin surface, and second, we also study the influence of the jet path relative to the orientation of muscle fibers. While most commercial jet injectors employ a fitting that would render the device normal to the skin surface, recent studies have proposed oblique injections, which may be beneficial for intradermal or subcutaneous tissue injection. Furthermore, for deeper intramuscular injections, we propose that an angled jet path taking the muscle fiber orientation into account may result in a bolus or dispersion zone that is conducive to increased cellular uptake of the drug.

1. Introduction

Drug delivery, both for therapeutic and preventative means, has been largely unchanged since the first documented use of intravenous injection in the 17th century, leading to the advent of the hypodermic needle in the mid-19th century (Ball, 2006; Kotwal, 2005). Hypodermic needle and syringes remain the vanguard method of delivery for the low cost and adaptability (e.g., syringe volume, needle diameter and length, etc.). However, many people suffer needle phobia, making this an undesirable choice (Nir et al., 2004; Verrips et al., 1998). This is especially pertinent for patients requiring multiple consecutive or daily doses, such as insulin injections for diabetic patents, and progesterone oil injections for IVF treatments. In addition, hypodermic needle injections are subject to failure when the injection depth is incorrect (Soliman et al., 2018), and accidental needle-stick injuries (Kotwal, 2005; Kane et al., 1999; Mannocci et al., 2016).

These factors, along with the development of novel drug formulations such as nucleic acid vaccines (Liu, 2003; Kutzler and Weiner, 2008; Tan et al., 2020), which may be high-viscosity complex solutions, as well as the need for coupling injections with electroporation (to increase cellular uptake) (Broderick and Humeau, 2015; Prausnitz, 1999) has promoted the search for new delivery mechanisms. One candidate in this arena, especially for large volume delivery of injectables, are jet injectors (Mitragotri, 2006; Raviprakash and Porter, 2006), which use a pressurized liquid to expel a high-velocity jet from a narrow orifice. The impact pressure of the jet, typically O(10) MPa is sufficient to puncture skin and penetrate into tissue layers below. The total depth

of the jet puncture, resulting drug bolus size, and overall efficacy of the injection depends on several factors including, but not limited to, drug viscosity, delivery volume, orifice diameter and applied load, which have been extensively explored in previous studies (Schramm-Baxter and Mitragotri, 2004; Schramm-Baxter et al., 2004; Baxter and Mitragotri, 2005; Schramm and Mitragotri, 2002; Taberner et al., 2012; Grant et al., 2015; Park et al., 2015; Li et al., 2016; Schoubben et al., 2015a; McKeage et al., 2018a,b; Schoubben et al., 2015b; Mohizin et al., 2018; Zeng et al., 2019; Moradiafrapoli and Marston, 2017; Rohilla et al., 2019; Rohilla and Marston, 2019; Simmons et al., 2019; Marston and Lacerda, 2019; Rane and Marston, 2020; Rohilla et al., 2020; Rane et al., 2021; Rane and Marston, 2021; Rohilla et al., 2021).

In contrast, the effect of jet angle relative to the skin surface has only been subject to relatively few studies. Several such studies date back to the 1960's, where jet injectors were used to administer BCG vaccine and to perform Tuberculin skin tests. In particular, these papers detail the orientation of the jet either by using a device with an angled orifice (e.g., Hendrix et al. (1965), Dull et al. (1967) and Luby et al. (1967)) or by deliberate placement of the device at 30–45 deg with a pinched fold of skin (e.g., Griffiths et al. (1965)).

One recent study by Gao et al. Gao et al. (2021) proposed an angled jet for dental anesthesia; the effect of an oblique (angled relative to tissue surface) jet was to reduce 'regurgitation' (fluid rejection), and thus increase overall delivery efficiency. In addition, they showed that oblique injections significantly reduced the occurrence of bleeding and laceration. A review article by Weniger and Papania (2008) also

E-mail address: jeremy.marston@ttu.edu (J. Marston).

^{*} Corresponding author.

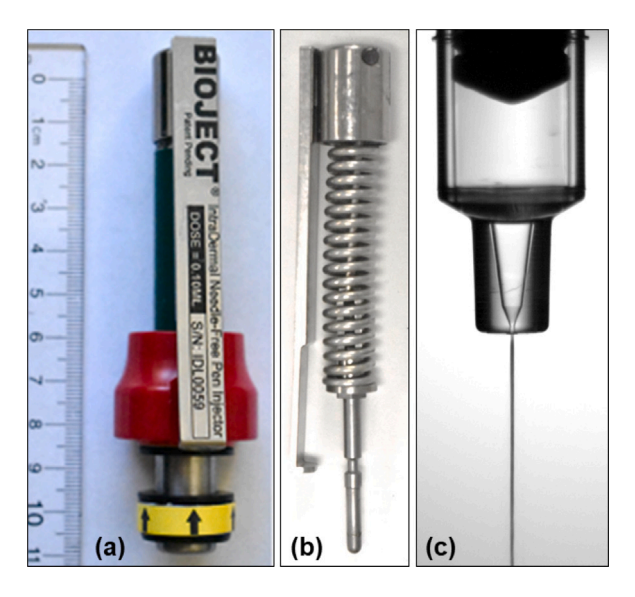


Fig. 1. Photographs of (a) the ID Pen injector device, and (b) inner spring-piston mechanism; (c) zoomed snapshot from high-speed video of the cartridge and jet.

documented specialized angled orifice nozzles used in older Multiple-Use Nozzle Jet Injector (MUNJIs) devices, such as the Ped-O-Jet®, for the purpose of intradermal vaccination.

Herein, we study the effect of oblique jet injections, motivated by both the results of Gao et al. Gao et al. (2021), and the hypotheses that (i) oblique injections can reduce injection depth and improve dispersion for intradermal injections, and (ii) oblique injections which account for muscle fiber orientation can provide optimal dispersion for cellular uptake in intramuscular injections.

2. Materials and methods

2.1. Jet injectors

The device used in this study was the Bioject ID Pen, capable of delivering 0.1 mL via an orifice with diameter of 0.157 mm. Photographs of the injector, spring and cartridge are shown in Fig. 1(a-c). These injectors employ cartridges designed for single-use (DCJIs), but herein we use modified re-usable cartridges. The actuation mechanism is a trigger-released spring-piston with a spring constant of 63 lbf/in, which results in a pressure-impulse stage in the first few milliseconds, followed by an approximate linear stage with a steady flow rate (nearly constant jet speed). The jet speeds were determined by high-speed video imaging and volumetric flow rate calculations, as detailed in previous publications (e.g., Rohilla et al. (2019)), as well as direct force measurements. In previous studies (e.g. Rohilla et al. (2019)) the effect of fluid rheology was studied, showing decrease in jet speed with increasing viscosity. However, many common injectates, including suspensions in phosphate buffer saline, are relatively low-viscosity. In addition, it is now known (e.g Williams et al. (2019), Rane and Marston (2024)) that viscous heat generation can significantly affect jet hydrodynamics, so for he present study, we focused on the most applicable, low-viscosity regime. As such, the liquid used as injectate for all cases was water with methylene blue dye (concentration \sim $2\%_{w/w}$) for visualization purposes.

2.2. Apparatus for oblique injections

To facilitate injections at a range of angles, a rigid holding clamp was 3-D printed using an i3 MK3S filament printer (Prusa Research, Czech Republic), which was mounted onto an optical railing system to

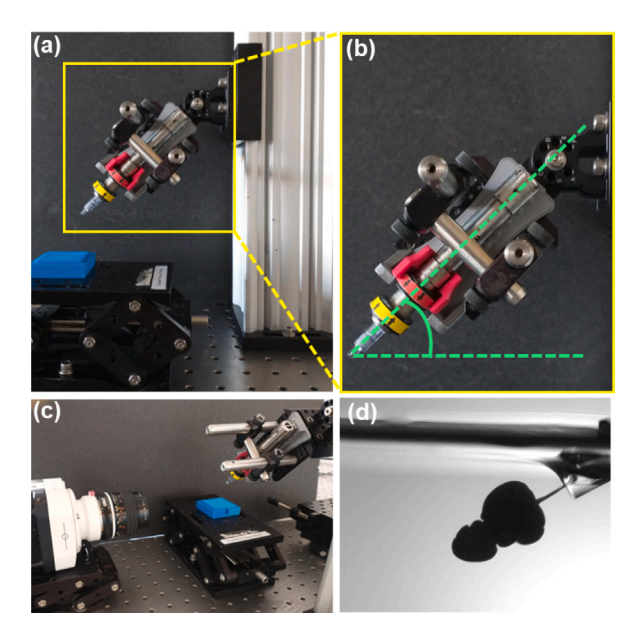


Fig. 2. Photographs of (a) the holding clamp and optical rail, (b) zoomed view defining the injector angle, and (c) overview of the high-speed imaging arrangement; (d) representative snapshot from high-speed video of injection into gelatin.

yield angles of 90° down to 30° in increments of 15° . This apparatus is shown in Fig. 2, along with the high-speed imaging arrangement and snapshot from injection into gelatin. Note that the angle of injection is defined as that relative to the horizontal (i.e. from the substrate surface), so that 90° implies the injector was perpendicular to the substrate/skin surface.

2.3. Tissue samples

To provide initial qualitative insights into the oblique jetting process, we used both tissue phantoms and ex-vivo tissue samples. The tissue phantoms were transparent hydrogels, made by mixing $5\%_{w/w}$ bovine gelatin powders in water, and allowing the gels to set overnight in small holding tanks (approx 8 cm \times 8 cm \times 8 cm). Given the size of the tanks, we cannot rule out wall effects. However, we did not observe any cases where the jet pierced deep enough to contact the container walls. Furthermore, although gelatin-based hydrogels are homogeneous, and therefore do not represent true tissue injections, such experiments can provide some insight into the dynamics and mechanisms that might be at play during jet injections. Prior studies (e.g. Rohilla and Marston (2019)) indicate that the elastic modulus of these gelatins is $G' \sim O10^1 - 10^2$ Pa.

For the ex-vivo tests we used porcine tissue procured from a local meat vendor, and human skin samples (purchased from NDRI) backed by porcine tissue. For the human skin tests, the injector cartridge tip was placed in an angled adapter to ensure contact with the skin using an applied normal load of 4.9 N (0.5 kg), as per previous studies (Rohilla et al., 2020). The liquid used in all cases was water with $2\%_{w/w}$ Trypan blue dye for visualization.

2.4. Imaging and quantitative measurements

To visualize the jet and injection for transparent hydrogel substrates, we used high-speed video cameras (Phantom V711 or M310) in combination with back-lighting and a diffuser screen to render high-contrast silhouette images. Typical frame rates used were around $8000{-}10,\!000$ fps, and effective pixel sizes were $\approx 20{-}30~\mu\text{m/px}.$ Video clips were then analyzed using Photron Fastcam Analysis software to track the plunger displacement (to render jet speed), depth of the

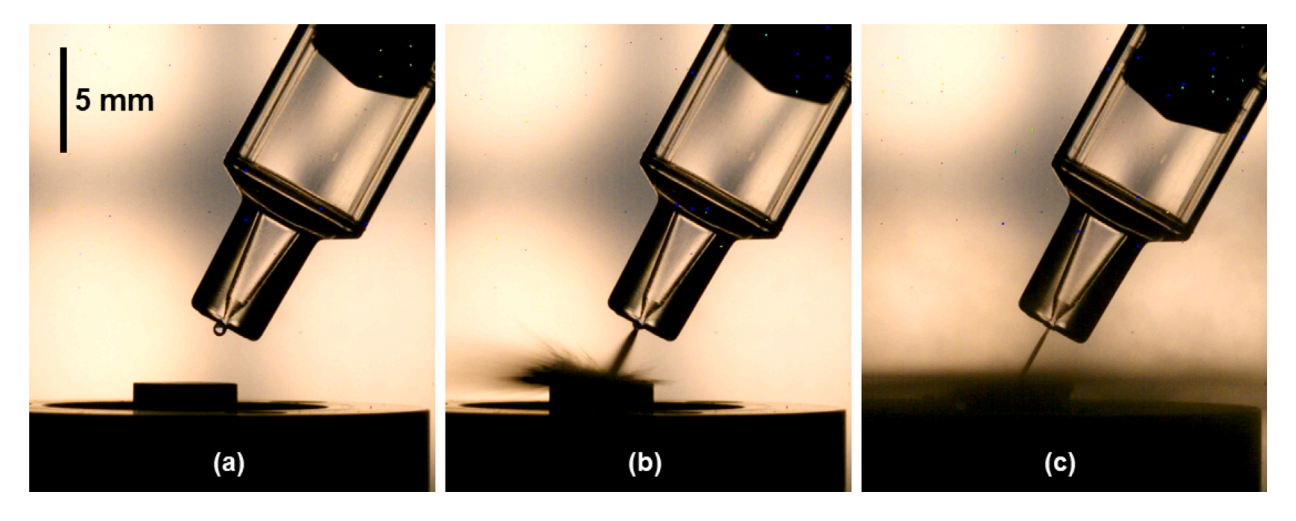


Fig. 3. Image sequence from high-speed video of water jet impacting the load cell depicting (a) initial configuration, (b) pressure impulse phase, and (c) steady jet phase.

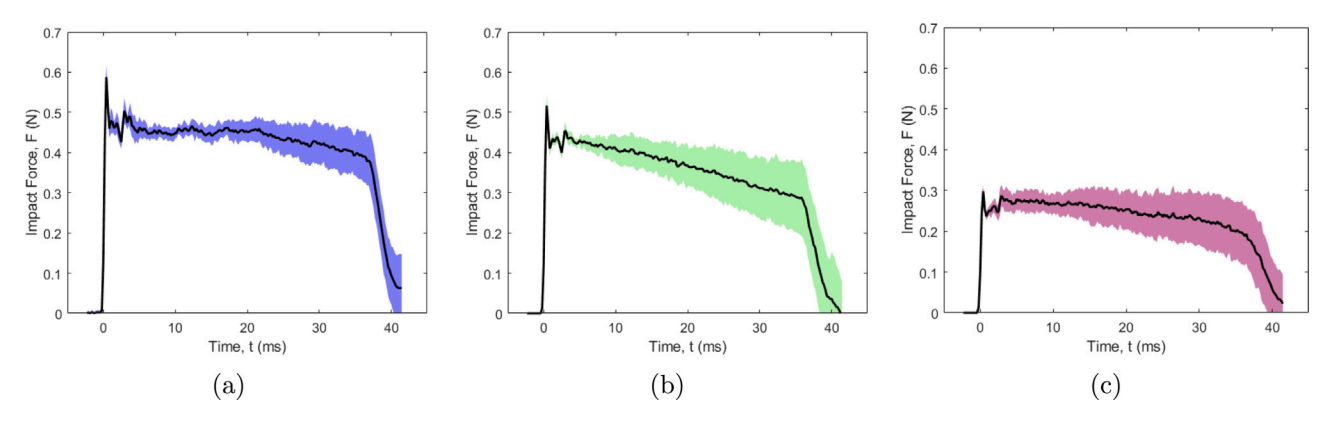


Fig. 4. Time-resolved jet impact forces for (a) 90-degrees, (b) 60-degrees, and (c) 30-degrees. The solid lines are the average of 5 trials, whilst the shading indicates one standard deviation (i.e., $\pm \sigma$).

injection over time, and extract the final bolus shape. For ex-vivo injections, the substrates were cut along the center of the injection point and imaged with a Digital SLR camera (Nikon D3400) to measure the final depth and dispersion width of the injection bolus. We also employed a miniature load cell (Futek LLB350, 50 lb) to determine the jet impact force for various angles.

3. Results and discussion

3.1. Jet impact forces

We begin our quantitative analyses with the jet impact forces, as measured by the load cell. An image sequence of the jet impacting the load cell is shown in Fig. 3. In particular, image (a) indicates the initial configuration prior to triggering the jet (t < 0, F = 0), image (b) indicates the impulsive pressure stage where the peak jet force occurs ($t \approx 0.3$ –0.4 ms, $F = F^*$), and image (c) indicates the steady jet stream (t \approx 3–37 ms, F : F^* \rightarrow F_{end}). When the spring-piston is triggered, the slamming of the piston with the rear-end of the plunger results in an impulse pressure and short-lived oscillatory phase, typically lasting less than 3-4 ms, as observed in the force profiles plotted in Fig. 4, before the system reaches an approximate linear motion. As the spring extends, the applied force decreases slightly, resulting in the gradual decline in force observed in all cases in Fig. 4 from $t \approx 3-37$ ms. At this time ($t \approx 37$ ms), there is a sudden decrease in force as the plunger reaches the end of the cartridge barrel, which identifies the end of injection.

From the jet duration, which is constant regardless of angles, we can estimate the mean jet speed from volumetric flow rate as $\bar{v}_i = V/(t_i A_o)$,

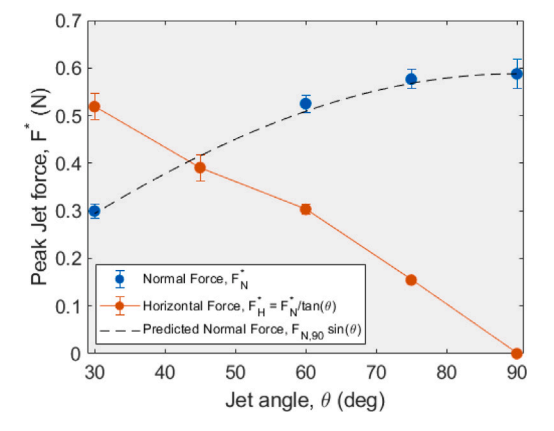


Fig. 5. Peak jet force, F^* , as measured by the load cell, resolved into normal and horizontal components. The black dashed line indicates the predicted normal force, $F^*_{90} \sin(\theta)$.

where V is the volume dispensed, t_j is the total jet time, and $A_o = \frac{\pi}{4} d_o^2$ is the orifice cross-sectional area. Using $t_j = 37$ ms, V = 100 µL, we find $\bar{v}_j = 139.6$ m/s, which is consistent with previous measurements on this device. However, as the jet angle is varied relative to the surface of the load cell, the force registered, which is the force normal to the surface varies according to $F_{90}^* \sin(\theta)$, where F_{90}^* is the peak force registered for 90-deg configurations.; this effect is shown is Fig. 5, where the normal force decreases from $F^* \approx 0.6$ to 0.3 N as the angle decreases

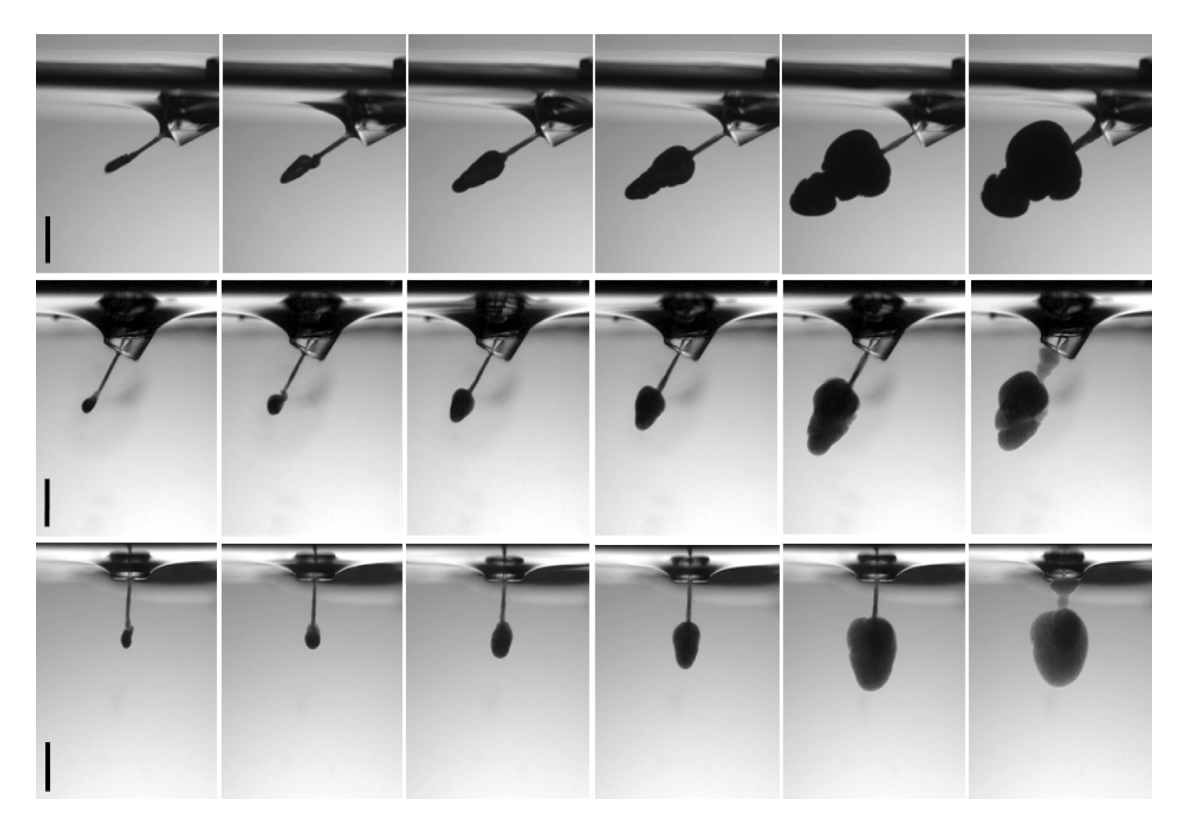


Fig. 6. Image sequences from high-speed video of water injected into 5% gelatin at $\theta = 30^{\circ}$ (top), 60° (middle), and 90° (bottom). The frames are taken at t = 1, 2, 5, 10, 30, and 85 ms, with the final frame (t = 85 ms) representing the final state. The scale bars represent 5 mm in all cases.

from 90° to 30°, but the tangential force increases from 0 to 0.5 N for the same range of angles. The total magnitude of peak jet force in all cases remains nearly constant, in the range 0.56–0.6 N, yielding peak jet speeds of $v_j^*=\sqrt{F^*/(\rho A_o)}\approx$ 170 m/s, whilst the jet speeds in the linear motion stage are $v_j\approx$ 141–147 m/s, in good agreement with those found using volume-based approach.

3.2. Injection into tissue phantoms

As a qualitative overview, Fig. 6 shows the injection process into hydrogel tissue phantoms at angles of 30° , 60° , and 90° . Since the injection volume and total jetting time is the same in all cases, the first 5 frames shown are taken at the same times from the start of the injection (t = 1, 2, 5, 10, 30 ms) showing penetration and growth of the bolus, whilst the last frame (t = 85 ms) are taken after the end of injection, when the gel is relaxing, and some fluid is expelled from the bolus due to elastic stress.

The final states at the end of injection are reproduced in Fig. 7, along with measurements of the total length from the orifice to the tip of the bolus (L^*) , and the corresponding vertical depth (Z^*) . Clearly, for the normal (90°) injection, $L^*=Z^*$, but for the angled configurations $(\theta<90^\circ)$ we have $Z^*\approx L^*\sin(\theta)$, implying the strict inequality $Z^*<L^*$. Note the approximation is due to fracturing and swelling of the bolus formation in the gelatin substrate. For the three realizations shown, we find that the total jet path lengths are $L^*=11.7$ mm, $L^*=12.3$ mm, and $L^*=15.9$ mm for the 90, 60, and 30-degree jets, respectively, whilst the vertical depth decreases from $Z^*=11.7$ mm to 10.7 and 7.95 mm respectively. This clearly demonstrates that as the angle increases, the jet penetrates through more tissue due to increased path length, but at a shallower depth relative to the skin. This conforms to the finding that the normal force component is reduced, so we would expect the jet puncture to remain shallow.

A summary of the jet path lengths and depths for the 5% gelatin substrates is presented in Fig. 8. Here, we observe that the reduction

in average depth from $\bar{Z}_{90}^*=11.7$ mm down to $\bar{Z}_{30}^*=9.6$ mm is less significant than the change in jet path length from $\bar{L}_{90}^*=11.7$ mm up to $\bar{L}_{30}^*=19.2$ mm. From a statistical standpoint, the effect of angle on total jet path length is highly significant (p<0.001), whilst the effect on depth (measured normal to the surface) is only moderately significant (p<0.1)

At first glance, this reduced total depth implies angled jet injection is more likely to result in intradermal (ID) and subcutaneous (SC) deposition, as opposed to intramuscular (IM), which could be beneficial for certain drug delivery objectives such as nucleic acid vaccination (targeting ID/SC) and therapeutics such as insulin injection (targeting SC). Moreover, the increased total jet path length implies that the jet and fluid contacts more total tissue, increasing the potential for improved cellular uptake.

3.3. Porcine tissue injections

To visualize the effect of orientation angle for jet injection simulating intramuscular injections, we used pork meat procured locally, then trimmed and cut to facilitate a range of experimental configurations. Fig. 9 provides illustrative images to demonstrate both the injection angle (i.e., the device angle from the surface of the tissue) and the jet path relative to the muscle fiber orientation. In our experiments, we defined 'normal' orientation when the jet path is opposed to the fibers and 'tangential' orientation when the jet path and fibers are aligned in the same direction, whilst the jet angle is defined relative to the surface of the tissue. In the representative examples shown, we observe that the bolus is an ellipsoid, whose major axis is always aligned with the orientation of the fibers. Moreover, we also observe that the jet path (and puncture depth) is reduced for normal orientation, but the effect is more clearly seen at 45-deg. A summary of the jet puncture depths is presented in Fig. 10, where it can be observed that the depth increases for tangential compared to normal, but this effect diminishes at 75-deg and 90-deg. The injections for normal configurations are

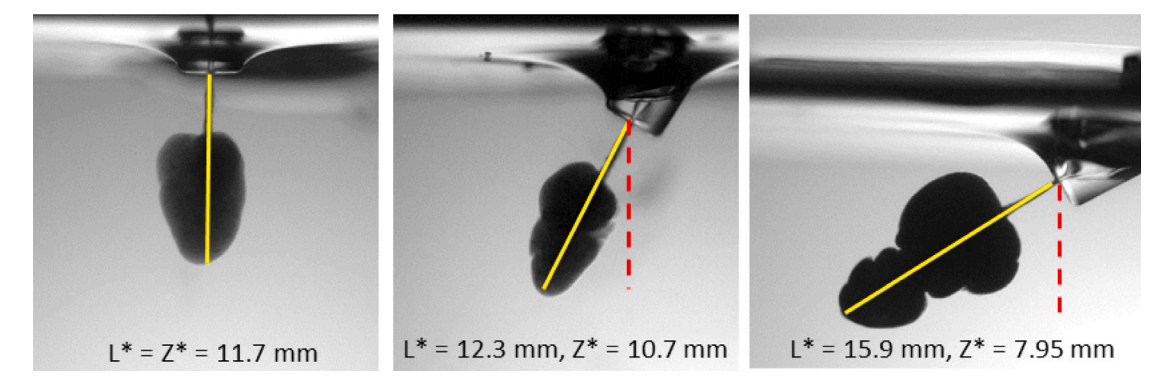


Fig. 7. Comparison of final bolus formations in 5% gelatin for 90, 60, and 30-deg angles. The solid yellow lines indicate the total distance from the orifice to the tip of the bolus (L^*) , whilst the dashed lines indicate the vertical depth (Z^*) .

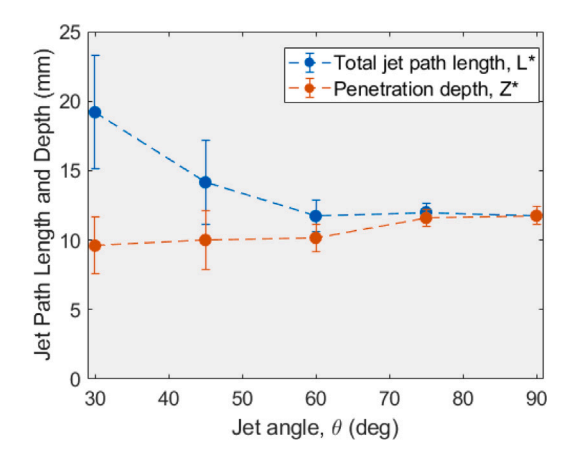


Fig. 8. Comparison of total jet path lengths (L^*) and vertical depths (Z^*) versus jet angle for $5\%_{w/w}$ gelatin substrates.

more consistent, evident from the smaller intra-sample ranges, and the total inter-sample variation is also relatively small (D=5–16.7 mm). In comparison, the tangential configuration shows larger intra- and inter-sample variation with the total range from D=5.8–29.5 mm. In particular, we observe the deepest punctures occurring for the $\theta=60^\circ$ 'tangential' configuration, which we hypothesize is due to the fact that the jet path is best aligned with the muscle fiber orientation in that configuration. This implies that IM injections should take into account the muscle orientation and flow direction of the injection device if a specific depth is being targeted. In general, a deeper jet path and/or distribution across a broader section of tissue could result in improved cellular uptake of vaccines, and reduced pressure (and hence pain) at the site of injection.

3.4. Human skin injections

A total of N=213 human skin injections were performed using skin samples procured from the National Disease Research Interchange (NDRI); for this study, we used skin from different anatomical locations (back, n=144; abdomen, n=69) as well as skin color (Black, n=71; White, n=75; Native American, n=67). The motivation for studying different skin colors stems from earlier reports (Luby et al., 1967; Wijsmuller and Snider, 1975) of intradermal injections, where it was found that the injected volume and the size of the skin wheal varied between males and females and between Black and White skin. As a specific example, jet injection of 0.1 mL of purified protein derivative (PPD)-S or (PPD)-G resulted in an average skin wheal diameter of approximately 4 mm for white males, but 6.5 mm for black males in Wijsmuller and Snider (1975). In contrast, the Mantoux technique

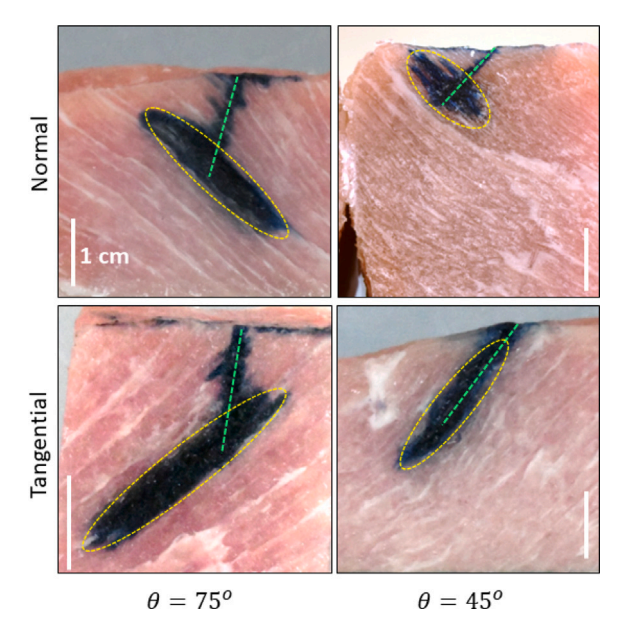


Fig. 9. Medial sections of pork loin injections for 0.1 mL water with $2\%_{w/w}$ Trypan blue dye. Angles (75 and 45-deg) are relative to the tissue surface, whilst the jet was aligned either normal (top row) or tangential (bottom row) to the muscle fibers in the tissue. The green dashed lines represent the assumed jet path, whilst the yellow ellipsoids outlines the bolus formed.

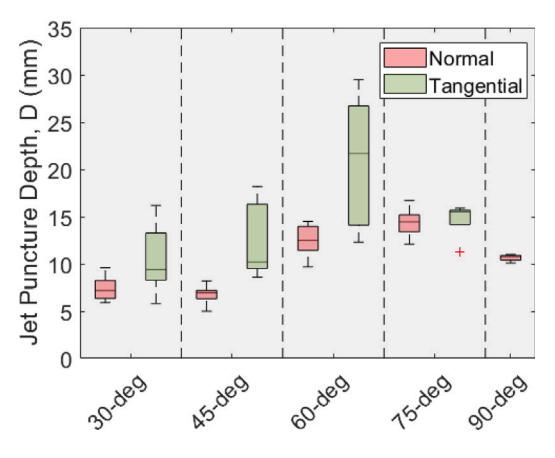


Fig. 10. Jet puncture depth versus angle for pork tissue. The orientations normal and tangential are as depicted in Fig. 9.

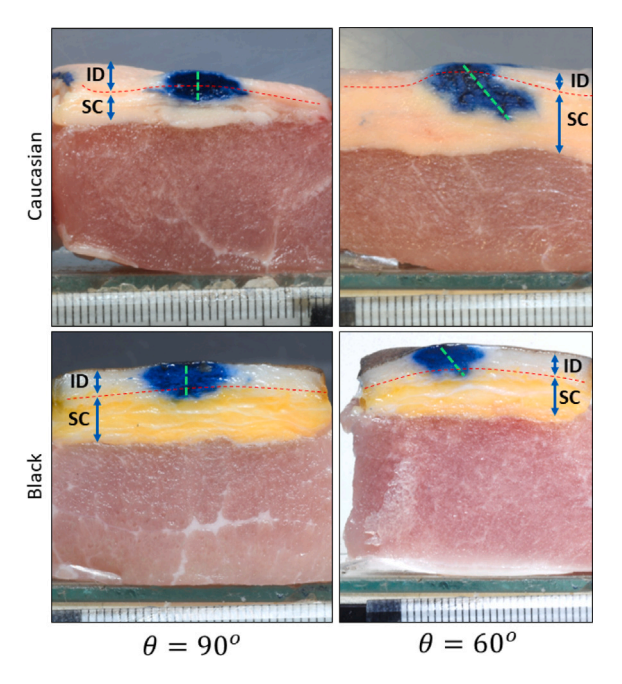


Fig. 11. Comparison of skin blebs formed by injection of 0.1 mL at either 90° and 60° with White (top row) and Black (bottom row) skin with fat tissue backed by pork tissue. The boundaries between ID and SC tissue are marked with red dashed lines, whilst the assumed jet path is marked with a green dashed line. Millimetric scales are at the bottom of each image.

resulted in skin wheals of 9 mm and 10.5 mm, respectively for the same groups. Since the authors of that study did not measure the injection efficiency (i.e., they did not quantify any rejection from the skin), it is unclear as to whether there was a higher rejection rate amongst the white males or whether the jet punctured deeper into the dermis and subcutaneous tissue. However, when considering the results of Luby et al. (1967), the mean injected volume was 0.051 mL for white skin and 0.065 mL for black skin, it is likely that the variation in skin wheals in Wijsmuller and Snider (1975) was due to differences in injection volume.

To provide a more realistic injection, we used skin samples with subcutaneous fat tissue and supported them with a 2–3 cm pork substrate. For all angles, the injector nozzle was fitted with a 25-mm adapter to maintain the jet angle, but also apply normal load of 0.5 kg to the skin, which is an important pre-requisite for successful ID injections, as concluded from earlier studies (Rohilla et al., 2020; Tran et al., 2023). For 45-deg only, we also performed a secondary set of experiments where the adapter was removed, and the cartridge nozzle was pushed directly onto the skin.

Fig. 11 shows photographs of the full tissue setup (skin with subcutaneous fat on top of pork tissue backing) with injections administered at both 90-deg and 60-deg into White skin (top row) and Black skin (bottom row). For reference, the ID-SC boundary has been marked by dashed lines in each, and the assumed jet path is also indicated in the images.

The fluid dispersion patterns (also referred to as skin 'blebs') in the dermal tissues form mostly oblate ellipsoids, with some fluid in the subcutaneous tissue. The fluid that enters the SC tissue may result either from direct jet penetration during the injection, or from diffusion after the injection. The blebs are typical of jet injections of 0.1 mL, as per previous studies (e.g., Baxter and Mitragotri (2005), Simmons et al. (2019) and Rohilla et al. (2020)), and the dye facilitates image analyses to determine the depth and width of the blebs, whilst rejected fluid mass (m^*) remaining on the skin enables estimates of the injection efficiency, i.e. the percentage of expelled fluid (V_{ej}) that correctly deposits under the skin, given as: $\eta = 100 \times (V_{ej} - m^*/\rho)/V_{ej}$.

Table 1

Anova summary (*p*-values) of main effects (jet angle, skin color, intradermal tissue thickness) on injection efficiency, depth and width of the blebs

Response	Response Effects			
recoponise				
↓	Jet angle	Anatomical Region	ID thickness	Skin Color
η (%)	1.72×10^{-10}	0.017	0.87	2.36×10^{-5}
D	3.26×10^{-8}	0.19	4.88×10^{-5}	9.5×10^{-3}
W	9.17×10^{-4}	0.85	4.1×10^{-4}	7.67×10^{-8}

Fig. 12 shows five repeat trials of injections administered into all skin types used herein (White, Black, Native American) at 90-deg. As evident from visual inspection, the injections are highly repeatable in all cases with primarily ID dispersion, and some SC diffusion. The average ID tissue thickness was 5 mm for the White skin (25 yr old, male, BMI 27.12), 1.7 mm for the Black skin (68 yr old, female, BMI 23), and 2.2 mm for the Native American skin (60 yr old, female, BMI 17) with all samples taken from the back region.

The injection depths, as measured from the top of the skin to the lowest point of the dye, were 9.23 \pm 0.36 mm, 5.22 \pm 0.34 mm, and 4.53 \pm 0.61 mm respectively, and the average injection efficiencies were 99.2%, 96.4%, and 97.7% respectively, indicating that injections performed at 90-deg are not just highly repeatable, but successful as measured by the amount of liquid actually deposited in the skin.

To understand the effects of jet angle, skin color and intradermal thickness in more detail, multiple repeat trials were taken for each configuration, and the summary data is presented in Fig. 13(a) and (b), for the injection efficiency and depth, respectively. For a breakdown of the data by skin type (color and anatomical location), the reader is referred to the supplemental materials. However, for brevity, we here just present the global trends; Assessing first the injection efficiency, it is obvious that jet angle has a significant effect with high efficiencies at 90-deg and 75-deg in most cases, evidenced by median values close to $\eta=100\%$, and decreasing efficiency as the angle decreases down to 45-deg.

We note, with reference to supplemental materials, the effect of jet angle is more evident for back tissues, whilst for abdominal tissues the injections were more consistent throughout. Although it is intuitive to attribute this to the thinner intradermal tissue, the full ANOVA results (see Table 1), indicate that it is likely due to an inherent property of the skin. As such, one possible explanation for the differences between the anatomical locations, i.e., back vs abdomen, could be differences in the tissue stiffness or orientation of Langer lines. Indeed the ANOVA results do indicate that anatomical region is significant.

As a final observation, when the adapter was removed, and the cartridge nozzle pushed directly into the skin at 45-deg (indicated as 45-deg* in Fig. 13), the efficiency improved again. This could be rationalized by the fact that when the cartridge nozzle is directly placed on the skin with 0.5 kg applied load, the injection essentially re-creates a 90-deg configuration, but the load is concentrated due to the smaller contact area, which results in more variation (as detailed in Tran et al. (2023)).

The injection depths, shown in Fig. 13(b) show more nuanced trends, but again indicating that 90-deg is the most consistent across skin samples from the back region (SI figure 2(a-d)), and less consistent for the abdomen region (SI figure 2(e,f)). In general, the depth decreases as the jet angle increases, as observed in the pork loin and hydrogel injections, and in all cases, the depths are representative of injections that have a combined ID-SC deposit.

From a categorical perspective, injections with over 90% delivery efficiency are considered successful (i.e., where 90% of the expelled volume actually deposits under the skin), so the overall efficacy of angled injections can be given in terms of successful vs. unsuccessful injections as a function of jet angle. The ensemble data for this is shown in Fig. 14, where it is clear that 90-deg is by far the most effective with success rate of 94%, dropping to just 26% at 45-deg. As observed in the individual data sets in Fig. 13, for the 45-deg configuration, if the end

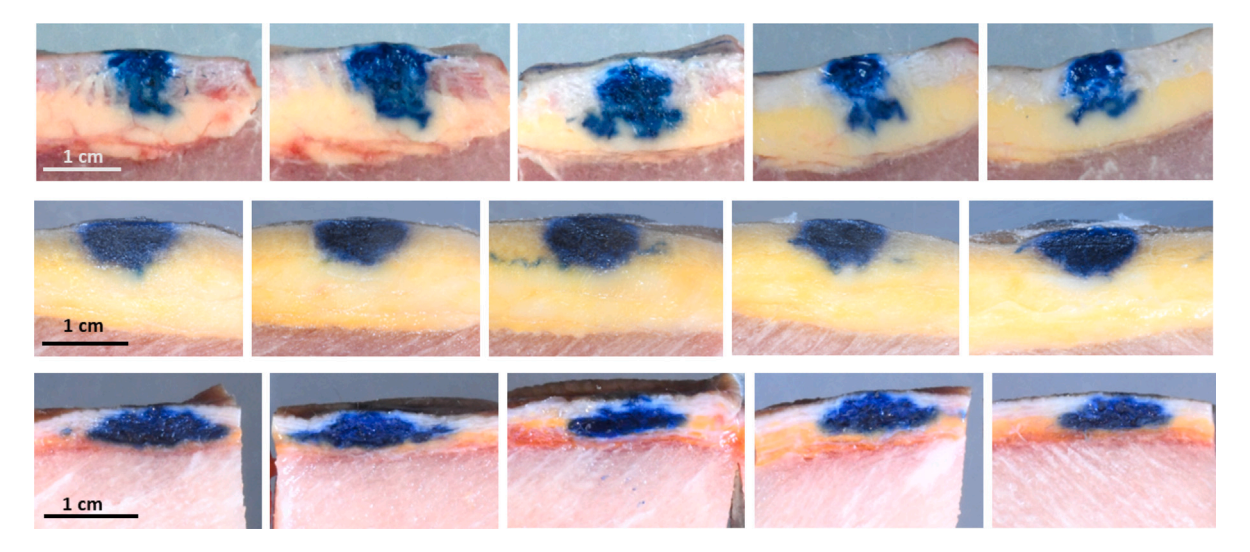


Fig. 12. Skin blebs formed by 90-deg injections of 0.1 mL into White skin (top row), Black skin (middle row), and Native American skin (bottom row) with 0.5 kg applied load, all indicating highly repeatable injections.

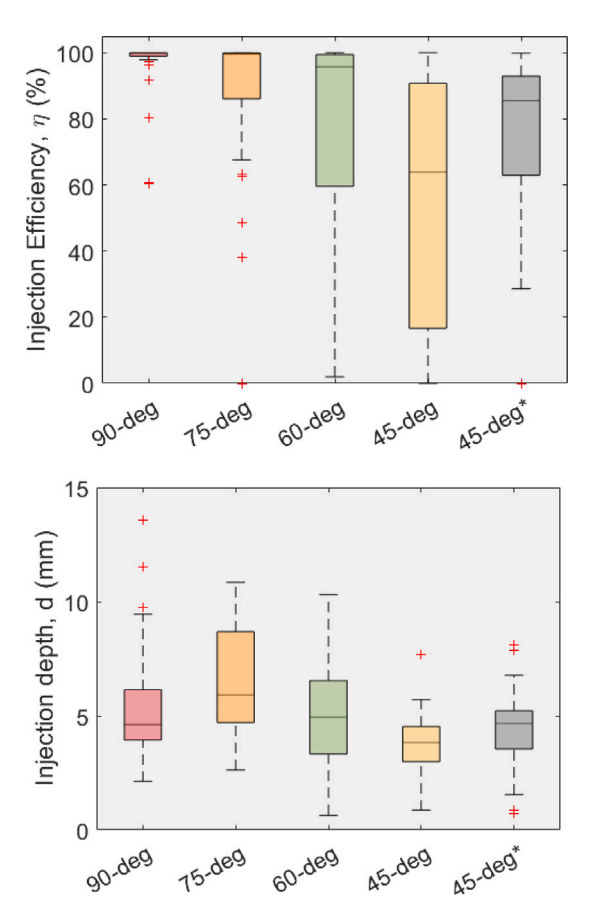


Fig. 13. Injection efficiency versus jet angle for all skin types.

attachment is removed so that the cartridge nozzle is pushed directly into the skin, the success rate increases, but only to 42%. As such, only the 90-deg configurations are deemed clinical viable.

As a final quantitative summary, a multi-factor ANOVA test was performed to determine the statistical significance of principal effects (jet angle, anatomical region, intradermal thickness, skin color) on the measured responses (efficiency, depth, width), and it was found that both jet angle and skin color are both highly significant factors (p < 0.01) for determining the injection efficiency and depth and

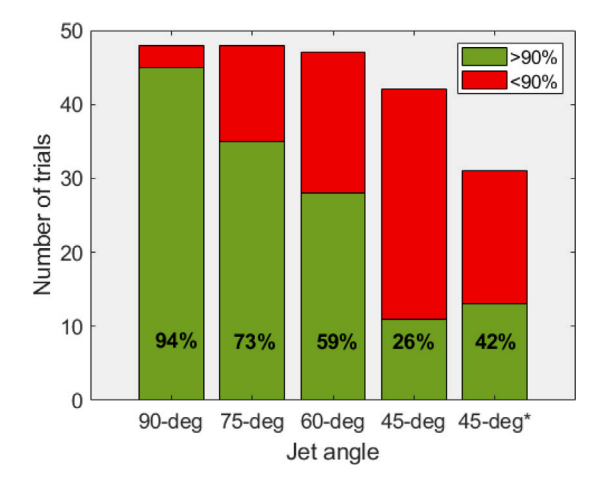


Fig. 14. Ensemble data across all skin injections (N = 213). Green indicates successful injections (i.e., > 90% fluid injected into skin), red indicates unsuccessful (i.e., < 90% injected). The final column labeled 45-deg* represents trials for the nozzle pushed directly into the skin without any end attachment.

width of the bleb. In contrast, the anatomical region of the skin was significant (0.01 < p < 0.05) for the injection efficiency, but insignificant (p > 0.05) for depth and width, whilst the intradermal tissue thickness was insignificant for efficiency, but highly significant for the depth and width. This infers that skin thickness is a controlling factor in the jet puncture depth and shape of the bleb formed, but it is not important for the efficiency. When considering that both skin color and anatomical region are significant factors, this implies that inherent properties of the skin tissue are more relevant than the thickness.

4. Conclusions and outlook

The study herein was motivated by the idea that angled jet injection could provide a means to control depth of drug deposition, and potentially result in increased cell transfection due to the broader dispersion within the intradermal tissue.

For hydrogel-based tissue phantoms, the total jet path length increased significantly from 11.7 mm to 19.2 mm as the jet angle decreased from 90 to 30-deg. However, the total depth (normal to the surface) was little changed decreasing from 11.7 mm to 9.6 mm. In

contrast, injections performed into porcine tissue exhibited more complex behavior, whereby the variation in puncture depth was dependent upon the jet orientation relative to the muscle fibers; it was found that the deepest penetration (typically 15–25 mm) was achieved with the 60-deg jet, since this angle coincided with the natural orientation of the fibers.

For injection into human skin, the effects of jet angle was found to be highly significant (p < 0.01) on all the primary responses – namely – injection efficiency, puncture depth, and dispersion width. The data exhibited general trends of decreasing puncture depth as the jet angle decrease, which supports the hypothesis of controlling depth. However, the significance of this result comes with the caveat that injection efficiency decreases dramatically as the jet angle is reduced from 90-deg to 45-deg. This is best understood by the ensemble data of success rates, as per fig. 15, where only the 90-deg jet has a success rate of > 90%.

In agreement with previous studies on Tuberculin skin testing (Dull et al., 1967; Luby et al., 1967), where an angled jet injector was used to inject 0.1 mL, skin color was also found to have a statistically significant effect (p < 0.01) on all the main responses. As also noted in the prior studies, the effect of thickness of the intradermal tissue was not significant on injection efficiency, thus it is hypothesized that the effect of skin color reflects an intrinsic property of the skin.

Some of the limitations of this study are as follows:

- The injection volume in this study was limited to 0.1 mL, based upon the original design and proposed use of the Bioject ID Pen. Some studies (e.g., Grant et al. (2015), McKeage et al. (2018a)) show effect of volume, thus it would be instructive to study jet angle for larger volume injections.
- 2. Although care was taken to prepare the hydrogel tissue phantoms and keep the samples hydrated, they could be subject to dehydration over time, at least within the upper section of these substrates once exposed to air, meaning that the top layer could present a slightly higher stiffness than the bulk.
- 3. The human skin samples are subject to a freeze-thaw cycle. Whilst this is not expected to significantly affect the intrinsic properties, it should be acknowledged there may be some difference with in-vivo tissue.
- 4. The effect of jet angle in this study did not consider the Langer lines (i.e., the inherent orientation of connective tissue fibers in the dermis) that may have played some effect on the human skin injections.

In summary, the effect of jet angle relative to the skin is significant. However, with regards to the injection efficiency (i.e., volume actually delivered) to the dermal tissues, the results herein clearly suggest a normal configuration (90-deg) is optimal. To be conclusive, this finding should be verified for larger volumes, different orifice diameters, and with various fluid viscosities.

CRediT authorship contribution statement

Idera Lawal: Writing – original draft, Methodology, Formal analysis, Data curation. Daniel de Castro Araujo Valente: Investigation, Data curation. Emil Khusnatdinov: Investigation, Data curation. Brian Elliott: Investigation, Data curation. Breanna Carruth: Investigation, Data curation. Clayton Penttila: Investigation, Data curation. Jeremy Marston: Writing – review & editing, Writing – original draft, Investigation, Funding acquisition, Conceptualization.

Declaration of competing interest

The authors declare the following financial interests/personal relationships which may be considered as potential competing interests: Jeremy Marston reports financial support was provided by National Science Foundation. If there are other authors they declare that they have no known competing financial interests or personal relationships that could have appeared to influence the work reported in this paper.

Data availability

Data will be made available on request.

Acknowledgments

The research reported in this paper was financially supported by the National Science Foundation (NSF), United States of America via Award number NSF-CBET-1749382.

Appendix A. Supplementary data

Supplementary material related to this article can be found online at https://doi.org/10.1016/j.ijpharm.2024.124612.

References

- Ball, C., 2006. The early development of intravenous apparatus. Anaes. Int. Care 34 (1), 22–26.
- Baxter, J., Mitragotri, S., 2005. Jet-induced skin puncture and its impact on needle-free jet injections: Experimental studies and a predictive model. J. Control. Rel. 106, 361–373
- Broderick, K.E., Humeau, L.M., 2015. Electroporation-enhanced delivery of nucleic acid vaccines. Expert Rev. 14, 195–204.
- Dull, H.B., Herring, L.L., Calafiore, D., Berg, G., Kaiser, R.L., 1967. Jet injector tuberculin skin testing: A comparative evaluation I. Methodology and results. Am. Rev. Respir. Dis. 97, 38–45.
- Gao, Q., Noel, G., Der Khatchadourian, Z., Taqi, D., Abusamak, M., Henley, A., Menassa, K., Velly, A., Emami, E., Mongeau, L., Tamimi, F., 2021. Needle-free injection: Dental infiltration anesthesia. Int. J. Pharm. 604, 120765.
- Grant, T.M., Stockwell, K.D., Morrison, J.B., Mann, D.D., 2015. Effect of injection pressure and fluid volume and density on the jet dispersion pattern of needle-free injection devices. Biosyst. Eng. 138, 59-64.
- Griffiths, M.I., Davitt, M.C., Brindle, T.W., Holme, T., 1965. Intradermal B.C.G. Vaccination by jet injection. Br. Med. J. 2, 399–401.
- Hendrix, C., Nicholes, C., Hursh, L., 1965. A new method of administering the tuberculin skin test. Am. J. Public Health 56, 818–820.
- Kane, A., Lloyd, J., Zaffran, M., Simonsen, L., Kane, M., 1999. Transmission of hepatitis
 B, hepatitis C and human immunodeficiency viruses through unsafe injections in the developing world: Model-based estimates. Bull. WHO 77, 801–807.
- Kotwal, A., 2005. Innovation, diffusion and safety of a medical technology: a review of the literature on injection practices. Soc. Sci. Med. 60, 1133–1147.
- Kutzler, M.A., Weiner, D.B., 2008. DNA vaccines: ready for prime time? Nat. Rev. Genetics 9, 776–788.
- Li, X., Ruddy, B., Taberner, A., 2016. Characterization of needle-assisted jet injections. J. Control. Rel. 243, 195–203.
- Liu, M.A., 2003. DNA vaccines: A review. J. Internal Med. 253, 402-410.
- Luby, J.P., Kaiser, R.L., Herring, L.L., Dull, H.B., 1967. Jet injector tuberculin skin testing: A comparative evaluation II. Quantitative aspects. Am. Rev. Respir. Dis. 97, 46–53.
- Mannocci, A., De Carli, G., Di Bari, V., Saulle, R., Unim, B., Nicolotti, N., Carbonari, L., Puro, V., La Torre, G., 2016. How much do needlestick injuries cost? A systematic review of the economic evaluations of needlestick and sharps injuries among healthcare personnel. Infect. Control. Hosp. Epidemiol. 37, 635–646.
- Marston, J.O., Lacerda, C.M.R., 2019. Characterization of jet injection efficiency with mouse cadavers. J. Control. Rel. 305, 101–109.
- McKeage, J.W., Ruddy, B.P., Nielsen, P.M.F., Taberner, A.J., 2018a. The effect of jet speed on large volume jet injection. J. Control. Rel. 280, 51–57.
- McKeage, J.W., Ruddy, B.P., Nielsen, P.M.F., Taberner, A.J., 2018b. Power-efficient controlled jet injection using a compound ampoule. J. Control. Rel. 291, 127–134.
- Mitragotri, S., 2006. Current status and future prospects of needle-free liquid jet injectors. Nat. Rev. Drug Discovery 5, 543–548.
- Mohizin, A., Roy, K.E.R., Lee, D., Lee, S.K., Kim, J.K., 2018. Computational fluid dynamics of impinging microjet for a needle-free skin scar treatment system. Comp. Biol. Med. 101, 61–69.
- Moradiafrapoli, M., Marston, J.O., 2017. High-speed video investigation of jet dynamics from narrow orifices for needle-free injection. Chem. Eng. Res. Des. 117, 110–121.
- Nir, Y., Paz, A., Sabo, E., Potasman, J., 2004. Fear of injection in young adults: Prevalence and associations. Am. J. Trop. Med. Hygiene 68, 341–344.
- Park, G., Modak, A., Hogan, N.C., Hunter, I.W., 2015. The effect of jet shape on jet injection. In: Proc. 37th Annu. Int. Conf. IEEE Eng. Med & Biol. Soc. pp. 7350–7353.
- Prausnitz, M.R., 1999. A practical assessment of transdermal drug delivery by skin electroporation. Adv. Drug Deliv. Rev. 35, 61–76.
- Rane, Y.S., Marston, J.O., 2020. Computation study of fluid flow in tapered orifices for needle-free injectors. J. Control. Rel. 319, 382–396.
- Rane, Y.S., Marston, J.O., 2021. Transient modelling of impact driven needle-free injectors. Comput. Biol. Med. 135, 104586.

- Rane, Y., Marston, J.O., 2024. Hydrodynamics of a dual-orifice needle-free jet injector. J. Drug Deliv. Sci Tech. 99, 105918.
- Rane, Y.S., Thomas, J.B., Fisher, P., Broderick, K.E., Marston, J.O., 2021. Feasibility of using negative pressure for jet injection applications. J. Drug Deliv. Sci. Tech. 63, 102395.
- Raviprakash, K., Porter, K.R., 2006. Needle-free jet injection of DNA vaccines: A brief overview and methodology. Methods Mol. Med. 127, 83–89.
- Rohilla, P., Khusnatdinov, E., Marston, J.O., 2021. Effect of air pockets in drug delivery via jet injections. Int. J. Pharm. 602, 120547.
- Rohilla, P., Lawal, I., Le Blanc, A., O'Brien, V., Weeks, C., Tran, W., Rane, Y., Khusnatdinov, E., Marston, J.O., 2020. Loading effects on the performance of needle-free jet injections in different skin models. J. Drug Deliv. Sci. Tech. 60, 102043.
- Rohilla, P., Marston, J.O., 2019. In-vitro studies of jet injections. Int. J. Pharm. 568, 118503.
- Rohilla, P., Rane, Y.S., Lawal, I., Le Blanc, A., Davis, J., Thomas, J.B., Weeks, C., Tran, W., Fisher, P., Broderick, K.E., Simmons, J.A., Marston, J.O., 2019. Characterization of jets for impulsively-started needle-free jet injectors: Influence of fluid properties. J. Drug Deliv. Sci Tech. 53, 101167.
- Schoubben, A., Cavicchi, A., Barberini, L., Faraon, A., Berti, M., Ricci, M., Blasi, P., Postrioti, L., 2015a. Dynamic behavior of a spring-powered micronozzle needle-free injector. Int. J. Pharm. 491, 91–98.
- Schoubben, A., Cavicchi, A., Barberini, L., Faraon, A., Berti, M., Ricci, M., Blasi, P., Postrioti, L., 2015b. Dynamics behavior of a spring-powered micronozzle needle-free injector. Int. J. Pharm. 491, 91–98.
- Schramm, J., Mitragotri, S., 2002. Transdermal drug delivery by jet injectors: Energetics of jet formation and penetration. Pharm. Res. 19, 1673–1679.
- Schramm-Baxter, J., Katrencik, J., Mitragotri, S., 2004. Jet injection into polyacrylamide gels: Investigation of jet injection mechanics. J. Biomech. 37, 1181–1188.

- Schramm-Baxter, J., Mitragotri, S., 2004. Needle-free jet injections: Dependence of jet penetration and dispersion in the skin on jet power. J. Controlled Rel. 97, 527–535.
- Simmons, J.A., Davis, J., THomas, J., Lopez, J., Le Blanc, A., Allison, H., Slook, H., Lewis, P., Holtz, J., Fisher, P., Broderick, K.E., Marston, J.O., 2019. Characterization of skin blebs from intradermal jet injection: Ex-vivo studies. J. Control. Rel. 307, 200–210
- Soliman, E., Ranjan, S., Xu, T., Gee, C., Harker, A., Barrera, A., Geddes, J., 2018. A narrative review of the success of intramuscular gluteal injections and its impact in psychiatry. Bio-Des. Manuf. 1 (3), 161–170.
- Taberner, A., Hogan, N.C., Hunter, I.W., 2012. Needle-free injection using real-time controlled linear Lorentz-force actuators. Med. Eng. Phys. 34, 1228–1235.
- Tan, X., Jia, F., Wang, P., Zhang, K., 2020. Nucleic acid-based drug delivery strategies. J. Control. Rel. 323, 240–252.
- Tran, W., Weeks, C., Y., Rane., Marston, J.O., 2023. Effect of nozzle shape and applied load on jet injection efficiency. J. Drug Deliv. Sci. Tech. 86, 104640.
- Verrips, G.H., Hirasing, R.A., Fekkes, M., Vogels, T., Verloove-Vanhorick, S.P., Delemarre-Van de Waal, H.A., 1998. Psychological responses to the needle-free medi-jector or the multidose disentronic injection pen in human growth hormone therapy. Acta Paediatr. 87, 154–158.
- Weniger, B.G., Papania, M.J., 2008. Alternative vaccine delivery methods. In: Plotkin, S.A., Orenstein, W.A., Offit, P.A. (Eds.), Vaccines, Fifth ed. pp. 1357–1392.
- Wijsmuller, G., Snider, D.E., 1975. Skin testing: A comparison of the jet injector with the Mantoux method. Am. Rev. Resp. Dis. 112, 789–798.
- Williams, R.M.J., McKeage, J.W., Ruddy, B.P., Nielsen, P.M.F., Taberner, A.J., 2019.
 Viscous heating assists jet formation during needle-free jet injection of viscous drugs. IEEE Trans. Biomed. Eng. 66 (12), 3472–3479.
- Zeng, D., Wu, N., Xie, L., Xia, X., Kang, Y., 2019. An experimental study of a spring-loaded needle-free inejctor: Influence of the ejection volume and injector orifice diameter. J. Mech. Sci. Tech. 33 (11), 5581–5588.